Two-dimensional gain cross-grating based on spatial modulation of active Raman gain*

Li Wang(王丽)[1,2], Feng-Xue Zhou(周凤雪)[1], Hong-Ju Guo(郭洪菊)[3], Yue-Ping Niu(钮月萍)[1], and Shang-Qing Gong(龚尚庆)[1,†]

[1] *Department of Physics, East China University of Science and Technology, Shanghai* 200237, *China*
[2] *School of Physics and Electronics Engineering, Nanyang Normal College, Nanyang* 473061, *China*
[3] *Shanghai Publishing and Printing College, Shanghai* 200093, *China*

(Received 27 November 2015; revised manuscript received 27 May 2016; published online 28 September 2016)

Based on the spatial modulation of active Raman gain, a two-dimensional gain cross-grating is theoretically proposed. As the probe field propagates along the z direction and passes through the intersectant region of the two orthogonal standing-wave fields in the x–y plane, it can be effectively diffracted into the high-order directions, and the zero-order diffraction intensity is amplified at the same time. In comparison with the two-dimensional electromagnetically induced cross-grating based on electromagnetically induced transparency, the two-dimensional gain cross-grating has much higher diffraction intensities in the first-order and the high-order directions. Hence, it is more suitable to be utilized as all-optical switching and routing in optical networking and communication.

Keywords: electromagnetically induced grating, gain cross-grating, active Raman gain

PACS: 42.50.−p, 42.50.Gy, 42.50.Nn , 42.81.Dp **DOI:** 10.1088/1674-1056/25/11/114205

1. Introduction

Based on electromagnetically induced transparency (EIT),[1–3] electromagnetically induced grating (EIG) is formed and has been investigated widely.[4–10] By replacing the coupling field with a standing wave, alternating regions of high transmission and absorption can be created, acting as a grating on which the probe beam can be diffracted. As shown in Ref. [4], when the probe field is resonant with the related states, EIG is a kind of amplitude grating which tends to diffract light into the central maximum, and the high-order diffraction efficiency is very low. If a high efficiency is desired for the high-order diffraction directions, detuning should be introduced. The detuning can cause a phase modulation to the probe beam and the formed phase grating then disperses energy into the high-order directions. However, the detuning gives rise to large absorption and the whole diffraction efficiency is lowered accordingly. Alternatively, electromagnetically induced phase grating (EIPG) based on the giant Kerr nonlinearity has been proposed to improve the first-order diffraction efficiency.[11,12] In the EIPG, a π cross-phase modulation across the probe beam with low energy loss has been accomplished. Furthermore, the effects of microwave modulation,[13] spontaneous generated coherence,[14,15] and static magnetic field[16] have also been considered to achieve improved diffraction efficiency in the first-order direction.

On the other hand, in the active Raman gain (ARG) systems, the probe field can be amplified and some related studies have been reported, such as superluminal light propagation,[17–19] ultraslow propagation,[20] rapidly responding nonlinear effects,[21–23] etc. A kind of gain grating that is based on the spatial modulation of ARG has also been proposed.[24–26] This kind of gain grating not only amplifies the zero-order diffraction intensity but it also effectively diffracts light into the high-order directions.

In our previous work, we have proposed a scheme for a two-dimensional electromagnetically induced cross-grating (EICG) based on EIT in a four-level tripod-type atomic system.[27] As two standing-wave fields along the x and y directions drive their corresponding atomic transitions, a two-dimensional EICG is created and diffracts light into the high-order directions. In order to improve the diffraction efficiency of the two-dimensional grating, in this paper we theoretically investigate a two-dimensional gain cross-grating (GCG) in a cold atomic medium, taking advantage of ARG. As the probe field propagates along the z direction and passes through the intersectant region of the two orthogonal standing-wave fields in the x–y plane, it can be significantly diffracted into the first-order direction and the zero-order diffraction intensity is also amplified. In contrast with the two-dimensional EICG, the first-order diffraction intensity of the two-dimensional GCG is greatly enhanced.

2. Atomic model and diffraction intensity distribution

We consider a four-level N-type cold atomic system as shown in Fig. 1(a). A Raman field with Rabi frequency $\Omega_{\rm r}$

*Project supported by the National Natural Science Foundation of China (Grant Nos. 11274112 and 11347133).
†Corresponding author. E-mail: sqgong@ecust.edu.cn
© 2016 Chinese Physical Society and IOP Publishing Ltd

drives the transition $|3\rangle \leftrightarrow |1\rangle$. A weak probe field with Rabi frequency $\Omega_{\rm p}(z)$ couples to the transition $|3\rangle \leftrightarrow |2\rangle$. The transition $|4\rangle \leftrightarrow |2\rangle$ is driven by a standing-wave field with position-dependent Rabi frequency $\Omega_{\rm s}(x,y)$. As shown in Fig. 1(b), the standing-wave field $\Omega_{\rm s}(x,y)$ is the combination of two orthogonal standing-wave fields with the same frequency, that is $\Omega_{\rm s}(x,y) = \Omega_{\rm s0}[\sin(\pi x/\Lambda_x) + \sin(\pi y/\Lambda_y)]$, where $\Omega_{\rm s0}$ is assumed to be real for simplicity, and Λ_x and Λ_y are the standing-wave field's spatial periods in the x and y directions, respectively. The probe field propagates along the z direction and passes through the intersectant region of the two orthogonal standing-wave fields in the x–y plane, while the Raman field may propagate along an arbitrary direction.

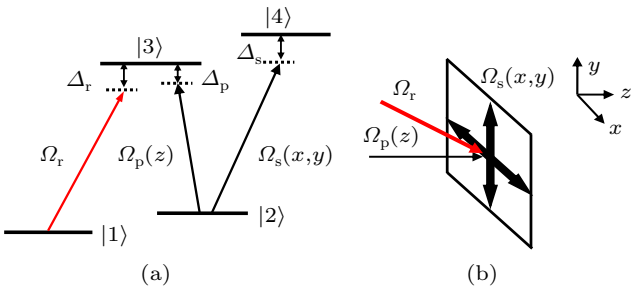


Fig. 1. (color online) (a) Schematic diagram of the four-level N-type atomic system. The possible levels correspond to the hyperfine levels of ^{85}Rb atoms: $|^5{\rm S}_{1/2}, F=3, m=-3\rangle = |1\rangle$, $|^5{\rm S}_{1/2}, F=2, m=-1\rangle = |2\rangle$, $|^5{\rm P}_{1/2}, F=2, m=-2\rangle = |3\rangle$, and $|^5{\rm P}_{3/2}, F=1, m=0\rangle = |4\rangle$. (b) Sketch of a prototype.

In the interaction picture, with the rotating-wave approximation and the electric-dipole approximation, the Hamiltonian is given by

$$H = -h[(\Delta_{\rm r}-\Delta_{\rm p})|2\rangle\langle 2| + \Delta_{\rm r}|3\rangle\langle 3| + (\Delta_{\rm r}-\Delta_{\rm p}+\Delta_{\rm s})|4\rangle\langle 4| + (\Omega_{\rm p}(z)|3\rangle\langle 2| + \Omega_{\rm r}|3\rangle\langle 1| + \Omega_{\rm s}(x,y)|4\rangle\langle 2| + {\rm h.c.})], \quad (1)$$

where $\Delta_{\rm p}$, $\Delta_{\rm r}$, and $\Delta_{\rm s}$ are the detunings of the probe field, the Raman field, and the standing-wave field, respectively. Here we consider the far-off-resonant Raman transitions, namely, $\Delta_{\rm r}$ and $\Delta_{\rm p}$ are much larger than the Rabi frequencies and the decay rates, and all of the atoms populate at the ground state $|1\rangle$ ($\rho \approx 1$) at the very beginning. By using the Liouville equation, we obtain the related density-matrix equations as follows:

$$\begin{aligned}
\dot{\rho}_{12} &= [{\rm i}(\Delta_{\rm p}-\Delta_{\rm r}) - \gamma_{21}]\rho_{12} - {\rm i}\Omega_{\rm p}\rho_{13} + {\rm i}\Omega_{\rm r}\rho_{32} - {\rm i}\Omega_{\rm s}(x,y)\rho_{14},\\
\dot{\rho}_{13} &= -({\rm i}\Delta_{\rm r} + \gamma_{31})\rho_{13} - {\rm i}\Omega_{\rm r} - {\rm i}g\rho_{12},\\
\dot{\rho}_{14} &= [{\rm i}(\Delta_{\rm p}-\Delta_{\rm r}-\Delta_{\rm s}) - \gamma_{41}]\rho_{14} + {\rm i}\Omega_{\rm r}\rho_{34} - {\rm i}\Omega_{\rm s}(x,y)\rho_{12},\\
\dot{\rho}_{24} &= -({\rm i}\Delta_{\rm s} + (\gamma_{41}+\gamma_{42}+\gamma_{21})/2)\rho_{24} + {\rm i}\Omega_{\rm p}\rho_{34},\\
\dot{\rho}_{32} &= ({\rm i}\Delta - (\gamma_{31}+\gamma_{32}+\gamma_{21})/2)\rho_{32} + {\rm i}\Omega_{\rm r}\rho_{12} - {\rm i}\Omega_{\rm s}(x,y)\rho_{34},\\
\dot{\rho}_{34} &= [{\rm i}(\Delta_{\rm p}-\Delta_{\rm s}) - (\gamma_{41}+\gamma_{42}+\gamma_{31}+\gamma_{32})/2]\rho_{34} + {\rm i}\Omega_{\rm p}\rho_{24} + {\rm i}\Omega_{\rm r}\rho_{14} - {\rm i}\Omega_{\rm s}(x,y)\rho_{32}, \quad (2)
\end{aligned}$$

where γ_{ij} is the atomic decay rate between levels $|i\rangle$ and $|j\rangle$. Under the weak-field approximation, we can obtain the steady-state solution ρ_{32} and then the linear susceptibility χ,[24]

$$\chi = \frac{3N_0\lambda_{\rm p}^3}{8\pi^2}\frac{\rho_{32}}{\Omega_{\rm p}}, \quad (3)$$

where N and $\lambda_{\rm p}$ represent the atomic density and the wavelength of the probe field, respectively.

In order to obtain the diffraction pattern for the probe field propagating through the medium, we begin with the Maxwell's equation. Under the slowly varying envelope approximation and in the steady-state regime, the propagation of the probe field driven by the atomic polarization can be described as

$$\frac{\partial\Omega_{\rm p}}{\partial z} = {\rm i}\chi\Omega_{\rm p}. \quad (4)$$

We assume that the interaction length of the cold atoms experienced by the probe field in the z direction is L. By solving Eq. (4), the transmission function for an interaction length L of the medium can be obtained as

$$T(x,y) = \exp(-{\rm Im}[\chi]L + {\rm i}\Phi), \quad (5)$$

where the first and the second terms correspond to the gain $(-{\rm Im}[\chi]L)$ and the phase modulation ($\Phi = {\rm Re}[\chi]L$). By performing the Fourier transformation on the transmission function and using the Fraunhofer diffraction theory, we obtain the Fraunhofer diffraction intensity distribution

$$I_{\rm p}(\theta_1,\theta_2) = |F(\theta_1,\theta_2)|^2 \frac{\sin^2(M\pi\Lambda_x\sin\theta_1/\lambda_{\rm p})}{M^2\sin^2(\pi\Lambda_x\sin\theta_1/\lambda_{\rm p})} \times \frac{\sin^2(N\pi\Lambda_y\sin\theta_2/\lambda_{\rm p})}{N^2\sin^2(\pi\Lambda_y\sin\theta_2/\lambda_{\rm p})}, \quad (6)$$

where M and N are the numbers of the spatial periods along the x and y axes of the grating illuminated by the probe beam, and θ_1 and θ_2 are the diffraction angles with respect to the x and y axes, respectively. Here the Fraunhofer diffraction of a single space period is

$$F(\theta_1,\theta_2) = \int_0^1 {\rm d}x \int_0^1 T(x,y)\exp(-{\rm i}2\pi x\Lambda_x\sin\theta_1/\lambda_{\rm p} - {\rm i}2\pi y\Lambda_y\sin\theta_2/\lambda_{\rm p})\,{\rm d}y. \quad (7)$$

The diffraction efficiency of the grating is taken to be the ratio of the intensity in the diffracted output to the intensity of the input. The probe diffraction intensity $I_{\rm p}(\theta_1, \theta_2)$ is normalized so that if $T(x,y) = 1$, then $I_{\rm p}(\theta_1, \theta_2) = 1$. The n-order diffraction efficiency is determined by Eq. (6) with $\sin\theta_1 = n\lambda_{\rm p}/\Lambda_x$ in the x axis and $\sin\theta_2 = n\lambda_{\rm p}/\Lambda_y$ in the y axis.

3. Results and discussion

In this section, we demonstrate the two-dimensional gain cross-grating and analyze the controllability of the diffraction efficiency. We assume $\gamma_{31} = \gamma_{32} = \gamma_{41} = \gamma_{42} = \gamma$, $\gamma_{12} = 10^{-3}\gamma$ with γ being the natural linewidth of state $|3\rangle$. L is given in

units of $\xi = 4\pi/3N_0\lambda_p^2$. Figure 2(a) displays the amplitude of the transmission function as a function of x and y. This shows that the probe field is amplified and the probe gain oscillates along the x and y directions in the periods of Λ_x and Λ_y, respectively. As shown in Ref. [24], the amplification of the probe field is attributed to the effect of ARG induced by the Raman field, and the probe gain is periodically changed due to the periodic intensity pattern of the standing wave in the x–y plane. In Fig. 2(b), we describe the normalized Fraunhofer diffraction intensity according to the transmission function of Fig. 2(a). An investigation of Fig. 2(b) shows that the probe field is not only amplified in the zero-order direction but also distributes significantly into the high-order directions. The first-order diffraction efficiency can approach 22%, which is much higher than that (2%) of the two-dimensional EICG.[27] Meanwhile, the dispersion of the probe field also changes periodically, and then the phase modulation of the probe field occurs along the x and y directions, as shown in Fig. 2(c). When the phase modulation is considered, a fraction of the zero-order diffraction intensity will deflect into the high-order directions and the first-order diffraction efficiency approaches to 24%, as shown in Fig. 2(d). In comparison with the two-dimensional EICG,[27] due to the ARG, the two-dimensional GCG has a much high diffraction intensity in the first-order direction.

In order to meet the requirement of ARG that most atoms populate in the ground state $|1\rangle$, we ensure that Δ_r and Δ_p are much larger than the Rabi frequencies and the atomic decay rates. Under this condition, we investigate the controllability of the first-order diffraction intensity of the two-dimensional GCG. Figure 3(a) depicts the effects of the Raman field's Rabi frequency on the first-order diffraction intensity. It is found that the first-order diffraction intensity increases with the increase of Ω_r, which is consistent with the one-dimensional gain-phase grating.[24] This can be explained by the gain and phase modulation as shown in Figs. 3(b) and 3(c). When the Raman field's Rabi frequency is small, the gain and phase modulation induced by the standing-wave field are not obvious due to the small probe gain and dispersion. With the

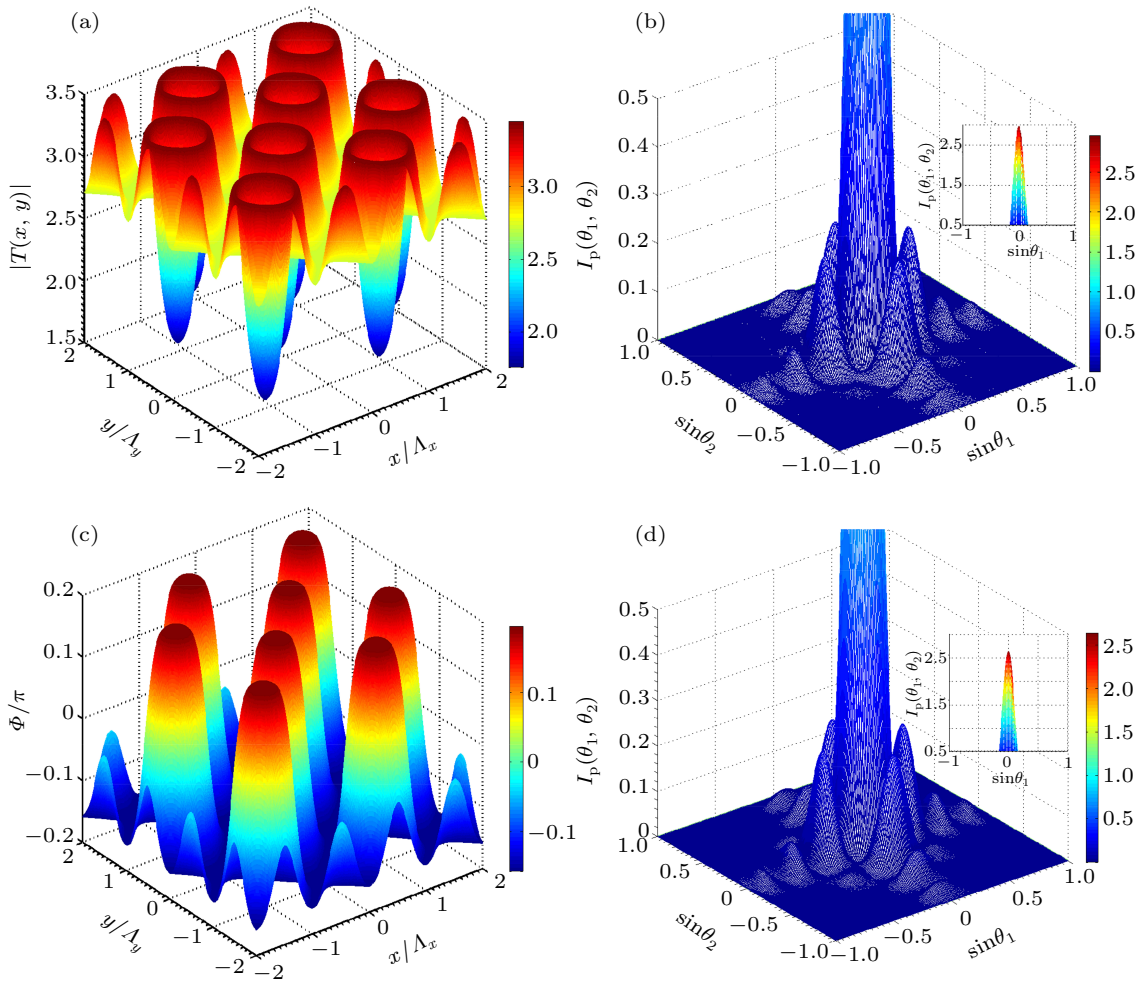


Fig. 2. (color online) The amplitude $|T(x,y)|$ (a) and the phase Φ/π (c) of the transmission function as a function of x (in units of Λ_x) and y (in units of Λ_y). (b) The normalized diffraction intensity $I_p(\theta_1,\theta_2)$ as a function of $\sin(\theta_1)$ and $\sin(\theta_2)$ for the corresponding transmission function shown in panel (a). (d) The two-dimensional gain cross-grating considers the gain and phase modulation. The insets in panels (b) and (d) show the residual parts of the diffraction patterns along $\sin(\theta_1)$. The parameters are $\Omega_r = 0.2\gamma$, $\Omega_{s0} = 0.2\gamma$, $\Delta_r = \Delta_p = 80\gamma$, $\Delta_s = 100\gamma$, $\Lambda_x/\lambda_p = \Lambda_y/\lambda_p = 4$, $L = 200\xi$, and $M = N = 5$.

increase of Ω_r, the probe gain and dispersion increase, which enlarges the gain and phase modulation depth and makes more light available for diffraction into the first-order direction. However, in our scheme, the Raman field's Rabi frequency cannot be set too large since the weak-field approximation for the probe field is applied in our numerical simulation. If the Raman field's Rabi frequency is too large, then the probe field will be amplified greatly and even exceed the other two fields. So we chose $\Omega_r = 0.2\gamma$ in the following simulations.

Figure 4(a) displays the first-order diffraction intensity as a function of Ω_{s0}. At small Ω_{s0}, the first-order diffraction intensity increases with Ω_{s0}. This is within our expectation. As shown in Figs. 4(b) and 4(c), with the increase of Ω_{s0}, the gain and dispersion are gradually enhanced at the individual antinodes, which increases the gain and phase modulation depth. As a result, more light can be diffracted into the first-order direction. However, the first-order diffraction intensity peaks at a certain Ω_{s0} ($\Omega_{s0} = 0.2\gamma$) beyond which it fades away. As Ω_{s0} increases further and exceeds 0.2γ, the phase modulation is always increased (see Fig. 4(c)) but the gain is gradually decreased at the individual antinodes and the gain modulation depth is also decreased, as shown in Fig. 4(b). So, light available for diffraction is reduced, and the first-order diffraction intensity decreases as $\Omega_{s0} > 0.2\gamma$ (see Fig. 4(a)). At the same time, we also investigate the effect of the interaction length L on the first-order diffraction intensity. It is obvious that the first-order diffraction intensity will increase with the increase of the interaction length L. In order to meet the actual experiment condition and the weak-field approximation of the probe field, the appropriate interaction length we chosen is $L = 230\xi$, which leads to an amplification of the probe field by a factor of four.[24] Therefore, due to the ARG, the two-dimensional GCG has a much high diffraction intensity in the first-order direction, and it has a great potential to be used as all-optical switching and routing[28] in optical networking and communication.

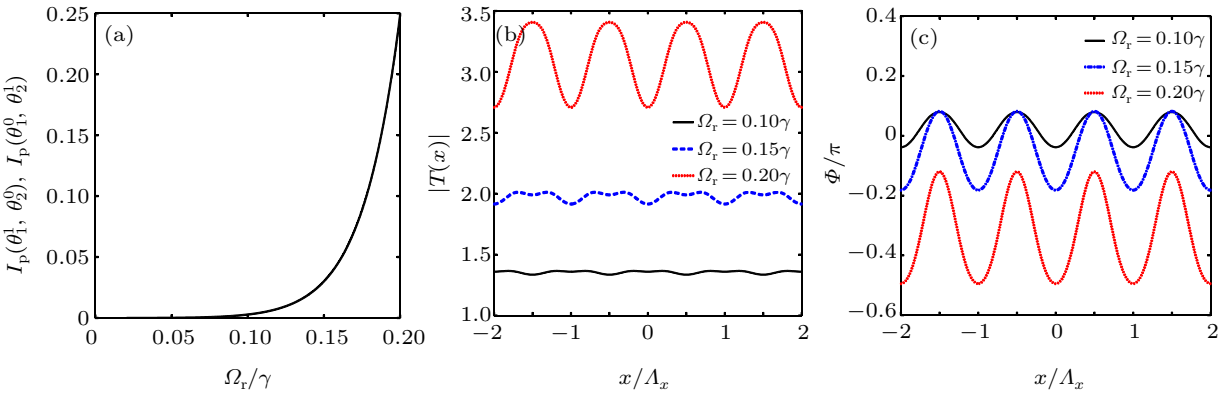


Fig. 3. (a) The first-order diffraction intensity $I_p(\theta_1^1, \theta_2^0)$ or $I_p(\theta_1^0, \theta_2^1)$ as a function of Ω_r. (b) The amplitude and (c) the phase of the transmission function in the x direction for different Ω_r at $y = 0$. The other parameters are the same as those in Fig. 2.

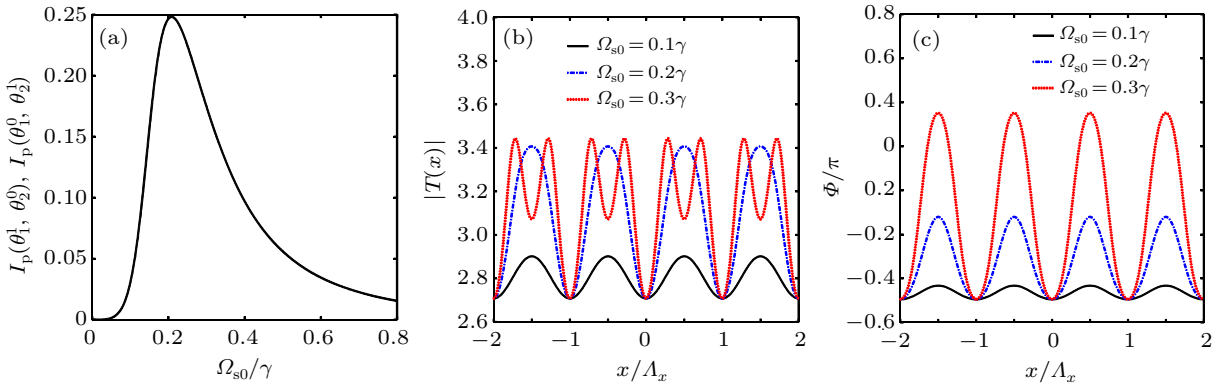


Fig. 4. (color online) (a) The first-order diffraction intensity $I_p(\theta_1^1, \theta_2^0)$ or $I_p(\theta_1^0, \theta_2^1)$ as a function of Ω_{s0}. (b) The amplitude and (c) the phase of the transmission function in the x direction for different Ω_{s0} at $y = 0$. The other parameters are the same as those in Fig. 2.

4. Conclusion

We theoretically demonstrate a two-dimensional GCG based on the spatial modulation of active Raman gain and dispersion in a four-level N-type cold atomic system. It is shown that not only the zero-order diffraction intensity is amplified but the first-order diffraction efficiency is also improved. As can be seen, it is mainly the probe gain that contributes to the gain modulation, while the phase modulation further improves the first-order and the high-order diffraction intensities. In comparison with the two-dimensional EICG, the two-

dimensional GCG has much high diffraction intensities in the first-order and the high-order directions. Thus it may be utilized as all-optical switching and routing, which are important optical devices in optical networking and communication.

References

[1] Harris S E 1997 *Phys. Today* **50** 36
[2] Yan X B, Gu K H, Fu C B, Cui C L and Wu J H 2014 *Chin. Phys. B* **23** 114201
[3] Zhang J, Zhang S, Ou B Q, Wu W and Chen P X 2014 *Chin. Phys. B* **23** 113701
[4] Ling H Y, Li Y Q and Xiao M 1998 *Phys. Rev. A* **57** 1338
[5] Mitsunaga M and Imoto N 1999 *Phys. Rev. A* **59** 4773
[6] Cardoso G C and Tabosa J W R 2002 *Phys. Rev. A* **65** 033803
[7] Dutta B K and Mahapatra P K 2006 *J. Phys. B* **39** 1145
[8] Dong Y B and Guo Y H 2014 *Chin. Phys. B* **23** 074204
[9] Yu S, Liao P, Yang Z Y and Gu W Y 2013 *Acta Phys. Sin.* **62** 22425 (in Chinese)
[10] Zhou F X, Qi Y H, Sun H, Chen D J, Yang J, Niu Y P and Gong S Q 2013 *Opt. Express* **21** 12249
[11] de Araujo L E E 2010 *Opt. Lett.* **35** 977
[12] Liu Y, Wang P and Peng S Y 2013 *Chin. Phys. B* **22** 104203
[13] Xiao Z H, Shin S G and Kim K 2010 *J. Phys. B* **43** 161004
[14] Wan R G, Kou J, Jiang L, Jiang Y and Gao J Y 2011 *Phys. Rev. A* **83** 033824
[15] Xie B, Cai X and Xiao Z H 2012 *Opt. Commun.* **285** 133
[16] Ba N, Wu X Y, Liu X J, Zhang S Q and Wang J 2012 *Opt. Commun.* **285** 3792
[17] Wang L J, Kuzmich A and Dogariu A 2000 *Nature* **406** 277
[18] Payne M G and Deng L 2001 *Phys. Rev. A* **64** 031802
[19] Agarwal G S and Dasgupta S 2004 *Phys. Rev. A* **70** 023802
[20] Jiang K J, Deng L and Payne M G 2006 *Phys. Rev. A* **74** 041803
[21] Deng L and Payne M G 2007 *Phys. Rev. Lett.* **98** 253902
[22] Jiang K J, Deng L, Hagley E W and Payne M G 2008 *Phys. Rev. A* **77** 045804
[23] Hang C and Huang G X 2010 *Opt. Express* **18** 2952
[24] Kuang S Q, Jin C S and Li C 2011 *Phys. Rev. A* **84** 033831
[25] Kuang S Q 2012 *Chin. Opt.* **5** 464
[26] Kuang S Q and Yang H G 2013 *J. Opt. Soc. Am. B* **30** 136
[27] Wang L, Zhou F X, Hu P D, Niu Y P and Gong S Q 2014 *J. Phys. B:At. Mol. Opt. Phys.* **47** 225501
[28] Ham B S 2004 *Appl. Phys. Lett.* **85** 893